https://doi.org/10.5194/os-2020-83
Preprint. Discussion started: 31 August 2020

Ocean Science
Discussions
Open Access
EGU

Sensitive dependence of trajectories on tracer seeding positions - coherent structures in German Bight surface drift simulations

Ulrich Callies[1]

[1]Institute of Coastal Research, Helmholtz-Zentrum Geesthacht, Max-Planck-Str. 1, 21502 Geesthacht, Germany

Correspondence: Ulrich Callies (ulrich.callies@hzg.de)

Abstract. Backward drift simulations can aid the interpretation of in situ monitoring data. Some trajectories, however, are sensitive to even small changes of the tracer release position. A corresponding spread of backward simulations implies convergence in the forward passage of time. Such uncertainty about the probed water body's origin complicates the interpretation of measurements. This study examines surface drift simulations in the German Bight (North Sea). Lines across which drift behaviour changes non-smoothly are obtained as ridges in the fields of the finite-time Lyapunov exponent (FTLE), a parameter used in dynamical systems theory to identify Lagrangian coherent structures (LCS). Results are shown to closely resemble those obtained considering a) two-particle relative dispersion and b) the average divergence of Eulerian velocities that tracers experience. Structures observed in simulated sea surface temperature and salinity further corroborate the FTLE results.

1 Introduction

In the German Bight area exists a comprehensive monitoring network, including the Marine Environmental Monitoring Network in the North Sea (MARNET), the Coastal Observing System for the North and Arctic Seas (COSYNA) and other stations. Details on the type of data being collected can be found in Baschek et al. (2017).Stanev et al. (2016) discuss issues related to modelling and data assimilation with spatiotemporal optimal interpolation. Multivariate statistical methods could also be used for optimizing the design of observational arrays (e.g. Chen et al., 2016; Kim and Hwang, 2020). However, data analysis based on a merely statistical description of spatial connectivity falls short of what can be achieved if hydrodynamic current fields from either models or remote sensing are available. This applies all the more, when it comes to the interpretation of data from a whole array of in situ monitoring stations.

Backward trajectories of Lagrangian tracers seeded at monitoring stations provide valuable insight into the background of water bodies that are probed (e.g. d'Ovidio et al., 2015). They help distinguish between temporal and spatial variability, i.e. local changes and advection from somewhere else. Because of considerable uncertainties, however, following just single particle trajectories is likely to be misleading. Trajectories accumulate deficiencies of the underlying hydrodynamic fields, including the effects of unresolved sub-grid scale hydrodynamic structures. Initially moderate deviations may possibly transfer

https://doi.org/10.5194/os-2020-83
Preprint. Discussion started: 31 August 2020

a trajectory to another submesoscale circulation structure. Backtracking water bodies from hypothetical monitoring stations in the vicinity of Helgoland, Callies et al. (2011, their Fig. 3) provide an example of how quasi-chaotic mixing may transform initially regular into quite contorted structures. Also in nature drifters released pairwise may separate quite fast (e.g. Callies et al., 2019; Meyerjürgens et al., 2020), which sets a limit to the reliability of simulations that can be achieved in the best case.

For these reasons, Lucas et al. (2016) for instance, studying the variation of bacterial community composition at station Helgoland Roads in the German Bight (North Sea), considered the behaviour of a whole bundle of backward trajectories, seeded within an extended region around the observational site. Uncertainties due to sub-grid scale eddies unresolved in the model were dealt with by a random walk component superimposed to each individual trajectory. This blanket approach implicitly deals also with the problem the present study focusses on: A possibly high sensitivity of backward trajectories (either simulated or observed) to where exactly they are seeded. A statistical measure for such particle spreading is relative dispersion, the mean square particle distance as function of time. LaCasce (2008) reviews how this parameter relates to the energy spectrum of a turbulent flow. Relative dispersion is called non-local if particle separation is dominated by eddies much larger than particle separation. In this case, characterized by a steep energy spectrum, particle separation is expected to grow exponentially. The very high sensitivity to initial particle positions implies what in dynamical systems theory is called chaotic advection.

Dynamical systems theory aims at a description of the kinematics of turbulent mixing. The approach is based on flow maps that describe particle advection over some time interval, according to Haller (2015) "*thereby mimicking experimental flow visualization by tracers*". This technique has widely been applied for analysing the microstructure of chaotic mixing processes in two dimensions (e.g. Pierrehumbert and Yang, 1993), describing how chaotic advection may transform initially small disks of fluid into complex filamentary structures. Trying to improve the sometimes vague definitions of such structures, Haller and Yuan (2000) introduced the framework of Lagrangian coherent structures (LCS). Their method seeks to identify material lines that function as only weekly permeable barriers for water body transport, attracting or repelling neighboured trajectories. Peacock and Haller (2013) provide a nice overview of the topic.

In case of flows with arbitrary time dependence, identification of LCSs can still be difficult. Hadjighasem et al. (2017) compare twelve candidate approaches that could be used. Among those, calculation of finite-time Lyapunov exponents (FTLE) is one of the most common methods. It is closely related to the finite-scale Lyapunov exponent (FSLE), originally introduced by Aurell et al. (1996, 1997) and used in experiments for diagnosing scale dependent separation rates between drifter pairs (LaCasce and Ohlmann, 2003; Sansón et al., 2017). Karrasch and Haller (2013), however, report some limitations for FSLE in LCS detection suggesting that an approach based on FTLE distributions may be more reliable. The FTLE fields are independent of an observer's reference frame (Haller, 2015), representing the rate at which neighbouring tracers diverge according to the largest eigenvalue of the so-called Cauchy-Green strain tensor. Ridges in the FTLE field are indicators of LCSs. Building on work by Haller (2001), Shadden et al. (2005) even define LCS in terms of these ridges, assuming that those approximately act as transport barriers. In to dimensions the LCSs are material lines transported with the flow.

Haller (2011) discusses examples in which substantial material flows crossing a FTLE ridge occur. It may also happen that a LCS does no produce a FTLE ridge or that a LCS suggested by FTLE does not exist. Therefore Haller (2011) developed a more sophisticated variational theory that also involves the eigenvectors of the Cauchy-Green strain tensor. Farazmand and

https://doi.org/10.5194/os-2020-83
Preprint. Discussion started: 31 August 2020

Haller (2012) present a corresponding numerical algorithm for two-dimensional application, based on the specification of strainlines along which exponential stretching occurs (to be distinguished from simple shear). Recently Tian et al. (2019) applied a variational method to identify the outer bounds of the Kuroshio current system.

Wiggins (2005) makes reservations that, as contrasted with many engineering applications, the presence and interaction of very different scales in geophysical flows can restrict the possibility of simulating detailed particle drift paths. The present study will therefore adhere to the simple conventional FTLE analysis. German Bight residual currents change with changing atmospheric winds (Schrum, 1997; Callies et al., 2017a) so that a description of exchange processes in a quasi-persistent hydrodynamic space-time structure like gyres or jets (Wiggins, 2005) is not the topic here. Analysing surface transports simulated by the operational hydrodynamic model BSHcmod, FTLE fields will be compared with statistical measures like single-particle absolute and two-particle relative dispersion, but also with the Lagrangian divergence (the average divergence that tracers experience along their trajectories (Huntley et al., 2015)). It turns out that all these parameters deliver very consistent results.

The paper is organized as follows: Section 2 first describes how Lagrangian drift simulations were performed based on pre-calculated hydrodynamic surface current fields. It follows a short compilation of the definitions of the FTLE, Lagrangian divergence and statistical measures of dispersion. Section 3 then reports three prototypical situations, evaluated also with regard to fields of sea surface temperature and salinity. Example trajectories illustrate the relevance of FTLE ridges as material separatrices. Three snapshots from a video available in the supplement illustrate the temporal variability of LCSs. A general discussion and a short summary conclude the paper.

2 Material and methods

2.1 Study area

The North Sea is a semi-enclosed shelf sea that connects to the north-eastern Atlantic at its northern boundary and through the English Channel at its southwest (Sündermann and Pohlmann, 2011). Strong tidal forcing occurs as a co-oscillation triggered by Atlantic tidal waves. This study focusses on the German Bight, the shallow south-eastern part of the North Sea with water depths of mainly 20-40 m, adjoining the Dutch, the German and the Danish coasts (Becker et al., 1992). In the German Bight, a mean cyclonic North Sea circulation corresponds with residual currents from the southwest to the north. Superimposed to this mean circulation, a strong weather driven variability occurs on short time scales (Schrum, 1997; Callies et al., 2017a). A fresh water plume emerging from the Elbe River and, to a minor extent, also the Weser river (see Fig. 1) can be observed as a permanent feature. Transient eddies and meanders depend on bottom topography, baroclinic instabilities and wind effects. The most important topographic feature is the old Elbe Glacial Valley, opening from today's Elbe estuary towards the northwest (west of Helgoland) into the open North Sea. Frontal structures depend on season but vary also on a short term basis (Budéus, 1989; Schrum, 1997). In the warm season, strong stratification occurs at water depths greater than approximately 30 m, mainly in the Elbe Glacial Valley. A baroclinic tidal mixing front (James, 1984; Holt and Umlauf, 2008) separates this region from the well-mixed more shallow coastal water, where stratification is prevented by strong tidal mixing (Krause et al., 1986).

https://doi.org/10.5194/os-2020-83
Preprint. Discussion started: 31 August 2020

2.2 Hydrodynamic fields

Offline drift simulations were based on surface currents taken from archived BSHcmod model output. Fields of surface temperature and salinity were taken from the same data base. BSHcmod is run operationally by the Federal Maritime and Hydrographic Agency (BSH). The model covers North Sea and Baltic Sea and is two-way nested with approximately 900 m resolution in the German Bight area and approximately 5 km in the open North Sea (Dick et al., 2001). In the vertical, a dynamical coordinate is used (Dick et al., 2008). The model's atmospheric forcing on an hourly basis is provided by the regional model COSMO-EU (Consortium for Small-Scale Modelling; Schulz and Schättler (2014)), run by the German Meteorological Service (Deutscher Wetterdienst – DWD). For an inclusion of wind stress, the parametrization by Smith and Banke (1975) is used. Stokes drift remains disregarded in archived operational model output.

In the process of archiving, BSHcmod hydrodynamic fields with originally higher vertical resolution were re-gridded. Conserving transport rates, this was done in such a way that the stored surface currents used in this study approximately represent the uppermost 5 metres of the water column.

2.3 Lagrangian drift simulations

Drift simulations were performed using the Lagrangian transport program PELETS-2D (Callies et al., 2011), based on BSHcmod model output archived on a 15 min basis. Originally, the PELETS toolbox developed at Helmholtz-Zentrum Geesthacht was designed for its use with hydrodynamic currents on unstructured triangular grids. Current fields provided on a regular grid (like those from BSHcmod) must be preprocessed, splitting each rectangular grid cell into two triangles. This transformation of grid topology does not affect the information content of hydrodynamic fields.

All simulations in this study were produced using the fourth-order Cash Karp method (Press et al., 1992) that belongs to the Runge Kutta family of solvers. It should be mentioned, however, that a simple Euler forward scheme used in other PELETS applications (e.g. Callies et al., 2011, 2017b, 2019) gave very similar results. The maximum time step is set to 15 min. Velocities are updated earlier if a tracer particle moves to another triangular grid cell.

2.4 Finite-time Lyapunov exponents (FTLE) as indicators of Lagrangian coherent structures (LCS)

Definition of the FTLE is based on a consideration of Lagrangian flow motions. A flow map Φ relates particle locations $\boldsymbol{x}_0$, where particles were seeded at time t_0, to their destinations $\boldsymbol{x}$ at later time $t = t_0 + \tau$:

$$\Phi_{t_0}^{\tau}(\boldsymbol{x_0}) = \boldsymbol{x}(t_0 + \tau; t_0, \boldsymbol{x}_0) \tag{1}$$

Taking the spatial gradient $\nabla \Phi_{t_0}^{\tau} = \partial \boldsymbol{x}(t_0 + \tau; t_0, \boldsymbol{x}_0)/\partial \boldsymbol{x}_0$, one obtains the following Cauchy-Green strain or deformation tensor (e.g. Shadden et al., 2005; Haller, 2015):

$$C(\tau; t_0, \boldsymbol{x}_0) = \left[\nabla \Phi_{t_0}^{\tau}(\boldsymbol{x}_0)\right]^T \nabla \Phi_{t_0}^{\tau}(\boldsymbol{x}_0) \tag{2}$$

https://doi.org/10.5194/os-2020-83
Preprint. Discussion started: 31 August 2020

This two-dimensional (in case of two-dimensional flows) tensor is symmetric and positive definite. Definition of the finite-time Lyapunov exponent is based on its largest eigenvalue λ_{max}:

$$\mathrm{FTLE}\,(\tau; t_0, x_0) = \frac{1}{\mid \tau \mid} \ln \sqrt{\lambda_{max}\,(C(\tau; t_0, \boldsymbol{x}_0))} \tag{3}$$

The absolute value of integration time τ is used because integration of particle drift can be conducted either forward or backward in time. The geometric interpretation of the FTLE refers to the maximum separation rate of neighbouring particles. Maximum separation among particles started on a small circle around location $\boldsymbol{x}_0$ occurs for those particles that end up along the largest principal axis of an ellipse that evolved from the initially circular structure (see Haller, 2015, his Fig. 4).

For the computation of FTLE fields, a regular Cartesian grid of tracers was released. Initial locations with 1 km resolution covered the German Bight area east of 6.5°E and south of 56°N (165 vortices in the longitudinal and 310 vortices in the latitudinal direction). The corresponding 51150 trajectories were integrated 250 hours backward in time (τ = -250 h). To avoid the computational burden of four additional close-by auxiliary trajectories, finite-differencing involved in FTLE specification (Eq. (2)) was performed involving trajectories seeded at neighbouring locations of the regular FTLE grid.

If at least one of the trajectories needed for FTLE calculation reached the coastline, the FTLE value was treated as missing. Corresponding gaps in the FTLE fields depend on prevailing atmospheric forcing. As BSHcmod covers the whole North Sea, no such problem occurs for particles that cross the open boundaries of the FTLE grid.

2.5 Finite-Domain Lagrangian Divergence (FDLD)

An incompressible two-dimensional flow field preserves the area of a Lagrangian patch during arbitrary deformations. In the present study this is not the case as the two-dimensional surface currents being used were extracted from 3D hydrodynamic fields, allowing for vertical exchange of water masses. Huntley et al. (2015) developed a concept that splits FTLE values into contributions that come from area-preserving stretching on the one hand and dilation on the other. With the area of a deformed elliptical Lagrangian patch being proportional to the product of the two eigenvalues λ_i of the Cauchy-Green strain tensor, Huntley et al. define a dilation rate Δ in a two-dimensional flow field as:

$$\Delta = \frac{\ln(\lambda_1 \lambda_2)}{\mid \tau \mid} \tag{4}$$

According to Huntley et al., this parameter equals the average Eulerian divergences experienced by a fluid parcel along its pathway. Hernández-Carrasco et al. (2018) refer to this integral parameter as the Finite-Domain Lagrangian Divergence (FDLD),

$$\mathrm{FDLD} = \frac{1}{\tau} \int_{t_0}^{t_0+\tau} \nabla \cdot \boldsymbol{v}(t', \boldsymbol{x}(t'))dt' \tag{5}$$

and demonstrate its potential for supporting the interpretation of satellite based observations of surface chlorophyll *a* patches. In the present study, FDLD values were calculated at all locations with valid FTLE values. Eulerian divergences needed for the evaluation of Eq. (5) were computed based on a discretization using auxiliary points at a 250 m distance. Velocities at these auxiliary locations were obtained by linear interpolation in the respective grid triangle.

https://doi.org/10.5194/os-2020-83
Preprint. Discussion started: 31 August 2020


Ocean Science
Discussions
Open Access
EGU

2.6 Absolute and relative dispersion

Absolute and relative dispersion are statistical measures for analysing Lagrangian data. Generally, absolute dispersion is defined as the second moment of the single particle displacement PDF, i.e. the variance of particle displacements relative to their starting position, which must not be confused with cloud variance (LaCasce, 2008). Ensemble averaging could be performed with respect to either different locations or different realizations at some fixed location. Here, following Haller and Yuan (2000), the simpler density of absolute dispersion is considered, describing just a single particle's squared displacement from its release point:

$$a^2(\tau; t_0, \boldsymbol{x}_0) = \mid \boldsymbol{x}(t_0+\tau; t_0, \boldsymbol{x}_0) - \boldsymbol{x}_0) \mid^2 \tag{6}$$

By contrast, relative dispersion describes the mean square separation of particle pairs with nearby initial release points. Relative dispersion at each node of the FTLE grid will be calculated combining information from four particle pairs,

$$D^2(\tau; t_0, \boldsymbol{x}_0) = \frac{1}{4}\sum_{i=1}^{4} \mid \boldsymbol{x}(t_0+\tau; t_0, \boldsymbol{x}_0) - \boldsymbol{x}(t_0+\tau; t_0, \boldsymbol{x}_0 + \delta\boldsymbol{x}_i) \mid^2 \tag{7}$$

where $\delta\boldsymbol{x}_i$ denotes the distance vector between neighbouring nodes. For a comparison with FTLE and FDLD fields, the logarithm of absolute and relative dispersion is a reasonable choice. Exponential growth of pair separations indicates the presence of Lagrangian chaos dynamical systems theory deals with (Wiggins, 2005).

3 Results

3.1 Examples

The following examples are intended to illustrate the occurrence of Lagrangian structures in German Bight surface currents. None of these structures are persistent, occurrence and specific details depend on the past evolution of environmental conditions.

3.1.1 First example

Fig. 1a shows the FTLE field for simulations initialized on 12 June 2015 (13:00 UTC) and extending over 250 hours backward in time. The scale was chosen to well visualize ridges of large values (negative logarithmic FTLE values have been plotted as if they were zero). All locations that gave rise to trajectories hitting the coast were disregarded.

At the time the plot refers to, the most prominent feature of the FTLE field is a south-north running ridge that separates the region of interest more or less into two halves. Further west, a less pronounced parallel second ridge occurs which, however, tends to be split into segments. Other more local and sometimes also weaker filamentary structures can be recognized. Intended to illustrate the physical relevance of the central FTLE-ridge, Fig. 1a includes three groups of four 250 h backward trajectories,

https://doi.org/10.5194/os-2020-83
Preprint. Discussion started: 31 August 2020

initialized in the wider neighbourhood of stations 1, 4 and 6 of the MARNET monitoring network[1]. To facilitate orientation and comparison, the six MARNET stations and the island of Helgoland (station H) will be indicated in all further figures.

The two pairs of hypothetical in situ stations (indicated by small circles, green and red) near MARNET stations 1 and 6 were located on either side of the central FTLE ridge. Simulations show a clear separation of trajectories emerging from different sides of the FTLE ridge. By contrast, trajectories started on the same side of the ridge (same colour) remain close to each other. Trajectory end points are indicated by small diamonds. The example trajectories illustrate how even close by in situ observations may encounter water bodies with a much different history. A complementary experiment considers four trajectories in the vicinity of MARNET station 4, with now all release points being located within the same contiguous region of low FTLE values. In this case all trajectories stay close together or even further converge.

[1]Station names: Deutsche Bucht (1), FINO1 (2), Ems (3), Nordseeboje III (4), Nordseeboje II (5), FINO3 (6)

https://doi.org/10.5194/os-2020-83
Preprint. Discussion started: 31 August 2020

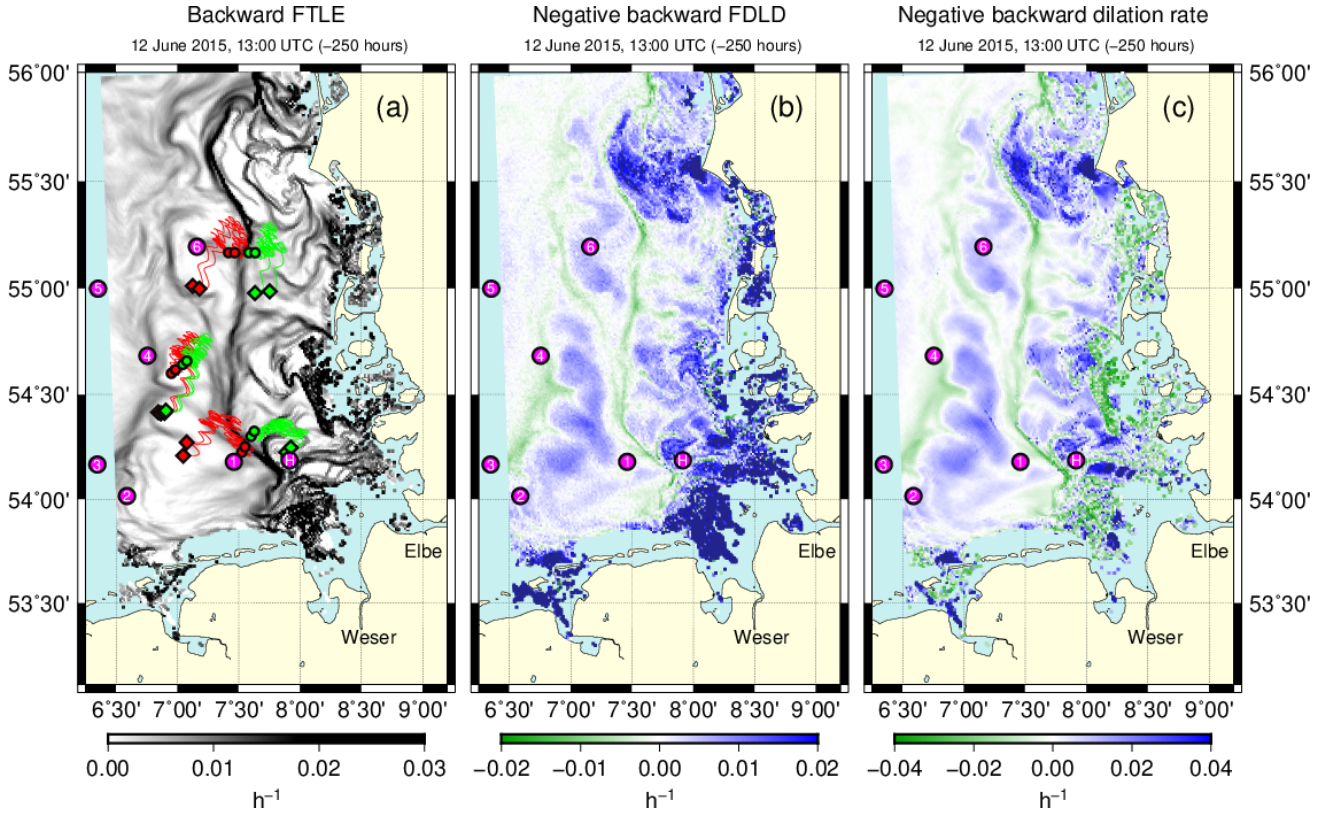

Figure 1. (a) FTLE field analysed for 12 June 2015 (13:00), based on trajectories calculated 250 hours backward in time. Example backward trajectories are shown, using different colours for better distinction. Trajectory release points are indicated by circles, small diamonds mark trajectory end points. Labelled circles (magenta) indicate locations of six stations of the MARNET monitoring network (labels 1-6) and of the island of Helgoland (label H). **(b)** Negative Lagrangian divergences (FDLD) calculated from Eq. (5) for all pixels that also appear in panel (a). Values exceeding the range covered by the colour scale are plotted in dark blue (positive, occurs near the coast) and dark green (negative, very few points). **(c)** Negative dilation rate Δ, calculated according to Eq. (4).

https://doi.org/10.5194/os-2020-83
Preprint. Discussion started: 31 August 2020

Divergence in backward time means convergence in ordinary forward time. Therefore, the negative backward Lagrangian divergence FDLD (Eq. (5)) shown in Fig. 1b is to be read in agreement with the usual passage of time. There is a striking structural similarity with Fig. 1a. Water parcels located on backward FTLE ridges have predominantly experienced converging surface currents along their pathway during the last 250 hours. Between these ridges there are wider regions with particles the history of which was dominated by diverging Eulerian currents.

Fig. 1c shows the field of dilation rate Δ, calculated according to Eq. (4). In the open sea, dilation rates deliver the same spatial structure as the FDLD in Fig. 1b, although the scale of values differs. This discrepancy in scale may be explained by numerical discretization and also the length of the integration interval which transforms small initial disks of the fluid into contorted structures rather than simple ellipses. More severe discrepancies occur near the coast, where even the signs of the analysed values differ. This deficiency presumably indicates that calculations based currents from a 5 m surface layer and with a 900 m horizontal resolution are inappropriate in these nearshore regions.

3.1.2 Second example

Fig. 2a shows a situation (26 March 2018, 18:00) in which the backward FTLE field is even more clearly partitioned, including also pronounced west-east oriented divides. FTLE ridges are particularly sharp, so that the simulated origins of water bodies located on either side of a FTLE ridge vastly differ. Example tracer trajectories illustrate this effect, assuming close by release points (red/green) on either side of FTLE ridges. Particularly large differences between backward trajectories occur for the most northern and the most southern of the three pairs.

https://doi.org/10.5194/os-2020-83
Preprint. Discussion started: 31 August 2020

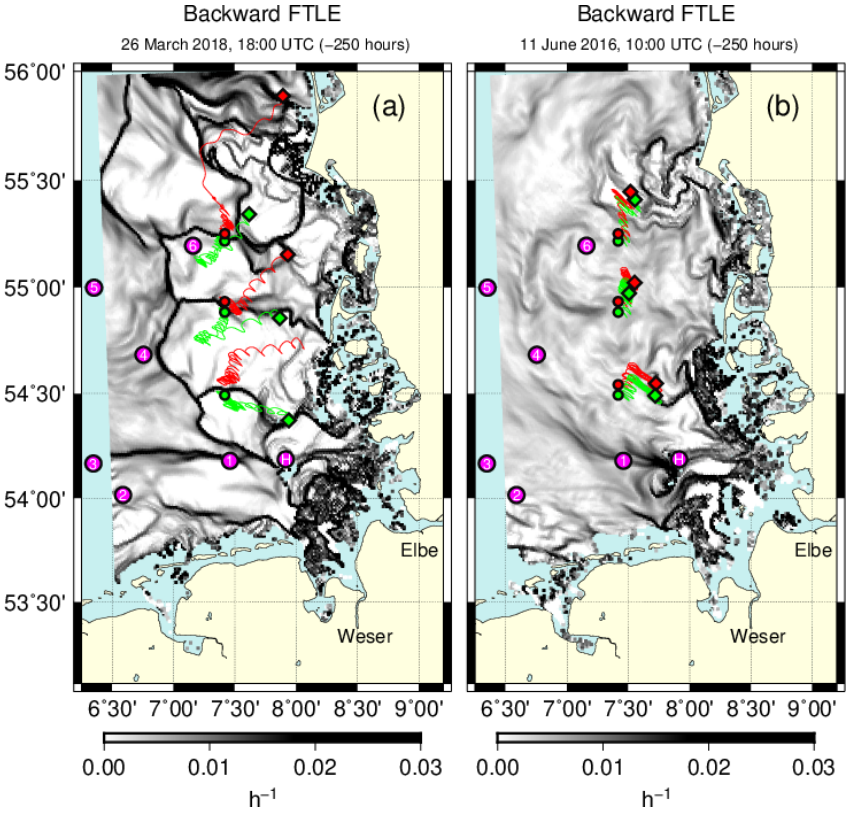

Figure 2. (a) Backward FTLE field (integration time 250 h) for 26 March 2018. Pairs of example trajectories were started on either side (green/red) of FTLE ridges. Trajectory release points are indicated by circles, end points by diamonds. Magenta circles indicate locations of MARNET stations (1-6) and of the island of Helgoland (H). **(b)** Example of a much smoother backward FTLE field on 11 June 2016. For the purposes of comparison, example backward trajectories were calculated from the same release points already used in panel (a).

https://doi.org/10.5194/os-2020-83
Preprint. Discussion started: 31 August 2020

Fig. 2b shows the example of a much less structured FTLE field. Overlaid to the FTLE field, the figure includes counterparts of the trajectories shown in Fig. 2a, released at exactly the same locations but on 11 June 2016 (10:00) rather than 26 March 2018 (18:00). Contrary to the situation in Fig. 2a, now all neighbouring trajectories closely resemble each other, just being shifted in agreement with shifted release points. A similar behaviour occurs at the time of Fig. 2a, if particles are released from the interior of a contiguous area delineated by the FTLE ridges (see Fig. S1).

3.1.3 Third example

The third example, referring to 29 February 2016 (11:00), provides an analysis in terms of statistical dispersion measures. Fig. 3a displays the spatial distribution of absolute dispersion. Remember that each pixel in the plot is calculated based on just one trajectory and represents the squared distance between the trajectory's release and end point. The plot reveals some sharp demarcations between zones with either broadly similar or at least smoothly changing drift velocities.

A measure that directly concentrates on small scale changes in drift behaviour is two-particle relative dispersion (Fig. 3b). Maps of absolute and relative dispersion are in very good agreement, relative dispersion highlighting sharp transitions in the graph of absolute dispersion. The two plots include the same example trajectories. Two test trajectories near the horizontal divide south of MARNET station 4 illustrate a stepwise change of advection speed, giving rise to the enhanced level of absolute dispersion for the test station located more to the south (green). Note that a pure change of drift direction, maintaining advection speed, would have affected relative but not absolute dispersion. Three additional magenta trajectories, seeded at MARNET stations 1, 2 and 6, were included to just visualize spatial variability of transports.

Finally, it is to be noted that the relative dispersion graph in Fig. 3b closely resembles the backward FTLE field (Fig. S2). FTLE ridges subdivide the area of interest in the same way as relative dispersion does, differences can hardly be distinguished.

https://doi.org/10.5194/os-2020-83
Preprint. Discussion started: 31 August 2020

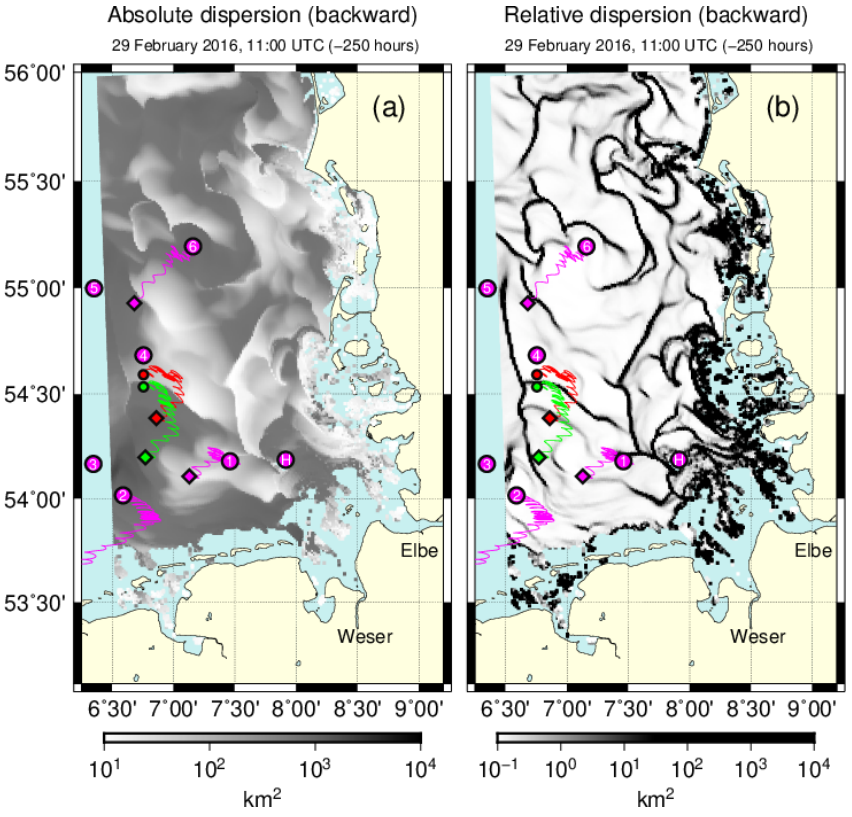

Figure 3. **(a)** Absolute dispersion (squared particle displacements) for 250 h backward integrations started on 29 Feb 2016 (11:00). Example trajectories were initialized at MARNET monitoring stations 1, 2 and 6 (magenta) and at two locations (red and green) neighbouring MARNET station 4 to its south. Small diamonds indicate each trajectory's final location. **(b)** Distribution of relative dispersion for the same situation.

https://doi.org/10.5194/os-2020-83
Preprint. Discussion started: 31 August 2020

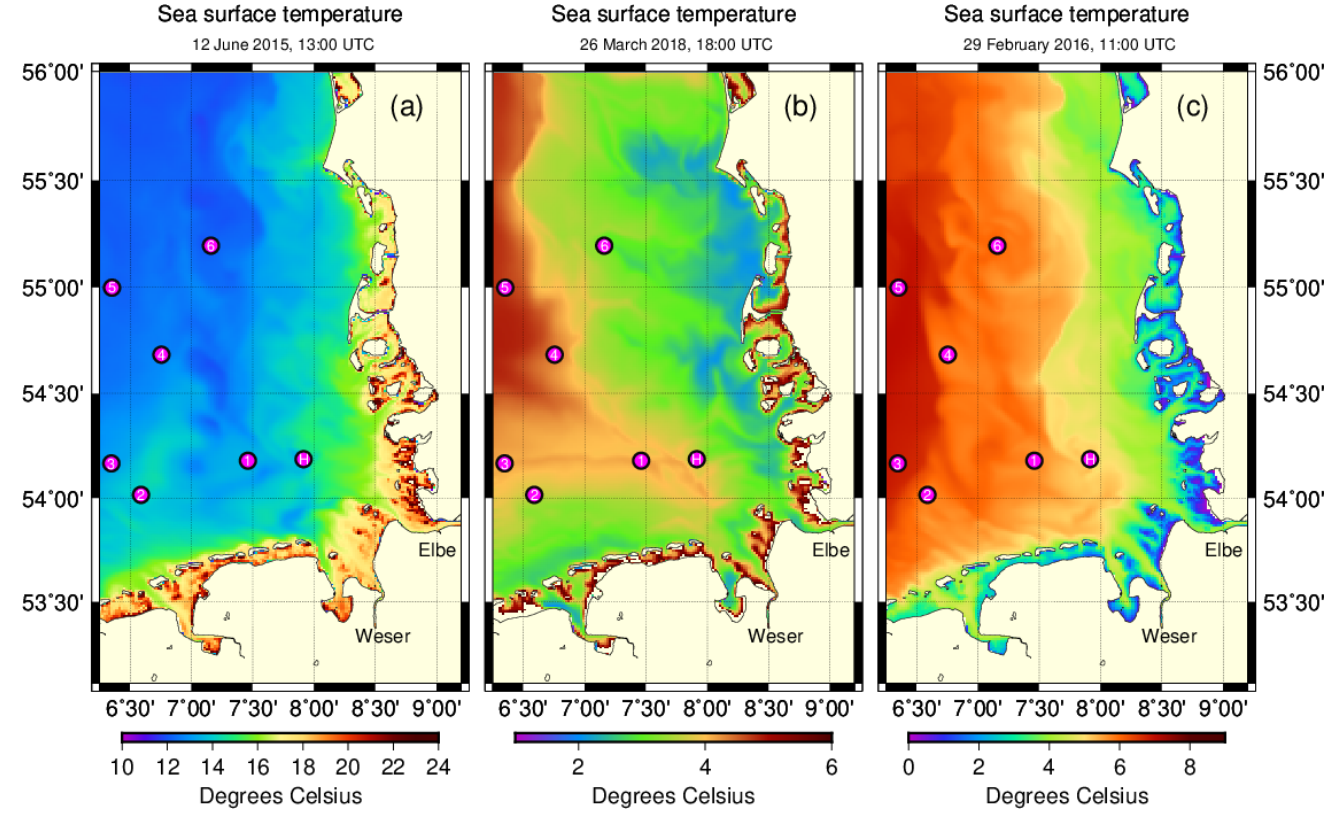

Figure 4. Sea surface temperatures at times the FTLE fields in Fig. 1 **(a)**, Fig. 2a **(b)** and the distributions of absolute and relative dispersion in Fig. 3 **(c)** refer to.

3.2 Surface temperatures

Studying the Agulhas current in the southwest Indian Ocean, van Sebille et al. (2018, their Fig. 3) found structures in fields of sea surface temperature (SST) that agreed with LCSs derived from geostrophic currents. For the German Bight region, Meyer-jürgens et al. (2020) found reduced relative dispersion for experimental drifters released in the vicinity of a tidal mixing front, indicating horizontal convergence in this region. This section addresses relationships between SST simulated in BSHcmod and the LCSs presented in the above examples.

https://doi.org/10.5194/os-2020-83
Preprint. Discussion started: 31 August 2020

Fig. 4a, referring to the situation in Fig. 1, shows a south-north oriented zone of relatively cool water. This belt is made up by a couple of patches that bear a striking structural resemblance to patches of positive divergence in Fig. 1b. These patches and the overall belt are delimited by the FTLE ridges shown in Fig. 1a. In the temperature field these lines of convergence (Fig. 1b) appear as being relatively warm. Fig. 1b suggests that some features of the temperature distribution in Fig. 4a can indeed be explained in terms of up- and downwelling.

Similar effects occur on 26 March 2018 (Fig. 4b, corresponding with Fig. 2a). The sharp west-east oriented ridges in Fig. 2a reappear in Fig. 4b as lines of relatively warm water (e.g. near MARNET station 6 or between MARNET stations 1 and 3). On the other hand, three tongues of relatively cool water extend westward from the coast into the areas between the lines of converging surface currents. Note that the eye-catching pronounced westward transition towards generally higher temperatures in the open sea (a transition broadly corresponding with increasing water depth towards the old Elbe Glacial Valley) does actually not always coincide with the main FTLE ridge neighbouring MARNET station 4. In particular to the north of this station, the FTLE ridge produces a line of relatively warm water that is clearly separate and shifted eastward (Fig. 4b).

Fig. 4c, showing the temperature field for 29 February 2016, corresponds with dispersion rates in Fig. 3. In this case, sharp transitions in the temperature field correspond with lines of large relative backward dispersion (Fig. 3b) or backward FTLE ridges (Fig. S2).

For all three examples addressed in Fig. 4, some related structures can be identified also in salinity fields (see Fig. S3). See Krause et al. (1986) and Budéus (1989) for a report on observations regarding the roles of temperature and salinity in different kinds of German Bight frontal structures.

3.3 Time evolution of coherent structures

FTLE (or dispersion) fields change continuously under changing environmental conditions. A video in the supplement, based on one FTLE field every 7 hours, shows the variability of FTLE ridges in the year 2016. The three panels of Fig. 5 were extracted from this video. They illustrate the development within the almost three week period 23 November to 12 December. Long FTLE ridges aligned in a meridional direction (Fig. 5a) evolve into a more cellular structure (Fig. 5c).

The FTLE field in Fig. 5b is much less compartmentalized than the fields in Figs. 2a and 3b, for instance. Instead, it contains more filamentary ridges that sometimes come very close. To illustrate the relevance of such narrow filaments, Fig. 5b combines a simulated backward trajectory starting at MARNET station 4 with another two trajectories (red and green) initialized slightly further east. Between the three seeding positions, FTLE ridges indicate enhanced backward particle separation (i.e. convergence in forward mode). Accordingly, the three trajectories end points are clearly much more separated from each other than tracers were at the outset. All three trajectories clearly reflect a reversal of the residual circulation that occurred during 22-24 November, when a pronounced cyclonic circulation changed to an anticyclonic circulation[2]. However, the more the observation position is shifted to the east, the more any hypothetical measurements would reflect conditions the probed water parcel experienced further south.

[2]see https://www.bsh.de/DE/DATEN/Stroemungen/Zirkulationskalender/zirkulationskalender_node.html

https://doi.org/10.5194/os-2020-83
Preprint. Discussion started: 31 August 2020

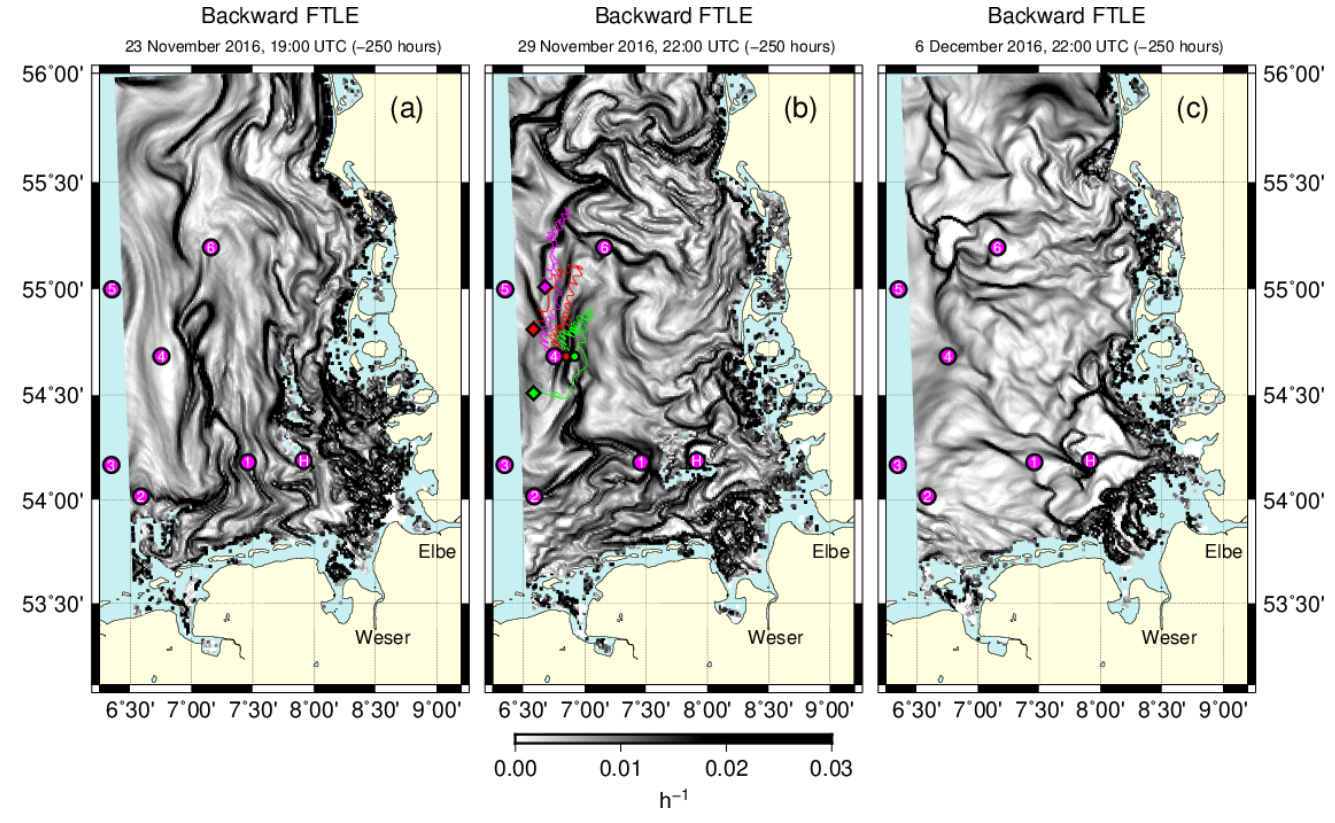

Figure 5. Example backward FTLE fields scheduled with nearly one week between them. Backward trajectories were started at MARNET station four (magenta) and two locations (red and green circles) on either side of the FTLE ridge further east. Small diamonds indicate trajectory end points. The three panels are extracted from a video available in the supplement.

https://doi.org/10.5194/os-2020-83
Preprint. Discussion started: 31 August 2020

4 Discussion

Taking a monitoring perspective, this study focussed on an analysis of attracting LCSs, technically identified as repelling LCSs in backward simulations. LCSs help delineate regions in situ observations are possibly representative for. A structure like the one shown in Fig. 1a, for instance, provides a warning that in the vicinity of the central south-north oriented FTLE ridge, even measurements at neighbouring locations might see water bodies with very different backgrounds. In Fig. 2a the FTLE ridges are surprisingly sharp, so that in this case even a small relocation of a measurement site could substantially shift the origin of water bodies being probed. Convergence of water bodies with different past histories introduces uncertainties in the interpretation of data. Ridges in the simulated backward FTLE field convey information on this uncertainty in a clear and amenable way.

Attracting LCSs, in dynamical systems theory also called unstable because of a fast stretching of particles along them (according to Harrison and Glatzmaier, 2010, an unfortunate historical definition), have been used for optimizing drifter deployments in field studies. Poje et al. (2002) proposed drifter deployment into attracting LCSs to ensure fast dispersal based on near-exponential material stretching, which lets drifters explore regions of high kinetic energy. Molcard et al. (2006) used this approach for assimilating drifter velocities into a ocean general circulation model. Different from these studies, Shadden et al. (2009) focus on repelling LCSs. Seeding drifters in a less localized way, Shadden et al. try to make drifters stay as long as possible in a specific region delineated by transport barriers.

Not looking into the future, backward FTLE fields can be simulated already at the time when observations are actually taken. Shadden et al. (2009) exemplify that a LCS's robustness might enable extrapolation of its separatrix function even beyond the time horizon of detailed operational hydrodynamic predictions, e.g. three days. Timely model based information on LSCs would allow for an adjustment of field campaigns to prevailing environmental conditions and data already gathered. New data should complement rather than duplicate information already available. Proper interpretation of measurements can much depend on both location and time when observations were taken. This is analogous to what Lekien et al. (2005) found in forward mode, trying to optimize a pollution release scheme based on forward FTLE fields. In this case favourable and unfavourable time spans for pollution release could clearly be distinguished from each other. Favourable time windows might also be identified when taking observations.

In this study, FTLE fields were analysed on a grid with 1 km resolution, nearly matching resolution of the underlying hydrodynamic current fields. Generally, defining FTLE fields on a finer grid to look at structures smaller than the resolution of the Eulerian hydrodynamic model would have been possible (see Huhn et al., 2012, for instance). Generated by chaotic advection with exponential material stretching rates, small scale structures arise from tracer simulations over distances much exceeding numerical grid resolution (Huhn et al., 2012). Generally, Harrison and Glatzmaier (2010) found locations of major LCSs to be fairly robust to spatial resolution.

According to Lekien et al. (2005), the relevance of FTLE ridges may be classified with regard to their length rather than the size of FTLE values. Here, LCSs often turned out to have considerable length and to be connected, sometimes forming a whole network of closed subregions. Throughout the study, all FTLE values were calculated based on trajectories integrated

https://doi.org/10.5194/os-2020-83
Preprint. Discussion started: 31 August 2020

250 hours back in time. This is roughly ten times the integration time Huhn et al. (2012) chose for their study in the Ria de Vigo estuary in Spain. Experiments reducing integration time to just 25 hours, revealed that key FTLE ridges tended to become less sharp but to not change their locations (not shown). This finding agrees with expectations (e.g. Peng and Dabiri, 2009; Shadden et al., 2009). According to Peng and Dabiri (2009), in practice integration time should be chosen such that it makes LCSs well resolved and clearly visible. As in Huhn et al. (2012), the tidal signal did not dominate the choice of integration time. The example trajectories shown, illustrate how changing residual currents, driven by wind forcing, play a major role for particle separation. This is very different in a Norwegian fjord, for instance, with topographically constrained currents driven mainly by tides (Orre et al., 2006).

Branicki and Malek-Madani (2010) warn that conclusions from two-dimensional FTLE fields could be misleading in shallow coastal waters with strong vertical mixing. Branicki and Malek-Madani see this point less critical when dealing with surface currents and buoyant Lagrangian tracers. Tracer convergence (divergence in backward FTLE fields) near FTLE ridges is consistent with an accumulation of drifting material near tidal mixing fronts (Simpson and Pingree, 1978; Thiel et al., 2011). If two-dimensional current fields are obtained from three-dimensional model output (as in this study), divergences may reflect injection of nutrients via vertical transports. This provides important input for modelling chlorophyll a dynamics, for instance. At the submesoscale, Hernández-Carrasco et al. (2018) found extreme divergence (indicating upwelling) and convergence (indicating accumulation of surrounding phytoplankton standing stocks) both being associated with phytoplankton patches observed in coastal waters.

In this study, analysed structures were remarkably consistent for fields of FTLE, FDLD, dilation rate or measures of dispersion. Differences between the FTLE and FDLD fields discussed by Huntley et al. (2015) could not be seen on the spatial scale considered. Fields of path-averaged finite-time Lagrangian divergence FDLD corroborate the role of backward FTLE ridges as lines of convergence (see Fig. 1). This relationship agrees with the results of many oceanographic studies. Olascoaga et al. (2013, their Fig. 1), for instance, provide an example of how a chlorophyll a plume in the Gulf of Mexico coincides with an attracting LCS. Lehahn et al. (2007) found satellite observations of chlorophyll filaments in the northeast Atlantic to well agree even with simulated geostrophic transports, contracting at and stretching along material lines. Referring to Lapeyre and Klein (2006), Lehahn et al. argue that an ageostrophic secondary circulation injecting nutrients from deeper layers may trigger further chlorophyll production.

Combining SeaWiFS ocean-colour data with altimetry-derived surface currents in the Brazil-Malvinas confluence zone, d'Ovidio et al. (2010) found that stirring by mesoscale currents can play an important role in structuring phytoplankton communities and even create what they call fluid dynamical niches, sharply delimited by LCSs. Hernández-Carrasco et al. (2018) study this topic at the submesoscale, using currents observed with High-Frequency Radar (HFR) in coastal waters. According to Scales et al. (2018) attracting LCSs can also be targeted by fisheries, lead by lines of drifting foam or debris. However, Abraham and Bowen (2002), employing the FTLE for estimating a stirring rate from surface velocity data in the East Australian Current region, emphasize that a model beyond a simple passive tracer concept would be needed to better understand chlorophyll distribution.

https://doi.org/10.5194/os-2020-83
Preprint. Discussion started: 31 August 2020

Relatively stable FTLE ridges connected to the island of Helgoland, for instance, could also be relevant for sedimentation processes. However, again an analysis of ideal passive tracer trajectories is likely to be too simplistic for studying such effects. Movements of inertial tracers can substantially differ from those of fluid parcels. Therefore the idea of LCSs has been generalized to include dynamics of inertial particles (Sapsis and Haller, 2009; Sudharsan et al., 2016; Günther and Theisel, 2017). This theoretical concept has successfully been applied on the scale of ocean eddies (Beron-Vera et al., 2015) but also on the very small scale of jellyfish feeding (Peng and Dabiri, 2009; Sapsis et al., 2011).

In this study, drift simulations were not validated against data. However, it was shown that to some extent the LCSs identified in model output manifested themselves also in simulated fields of surface temperature (Fig. 4) and salinity (Fig. S3) as intrinsic tracers. A relationship between frontal structures and FTLE ridges confirms the relevance of LCSs for surface current transports. Becker et al. (1992) summarize different types of fronts (river plume, thermal and upwelling fronts) that occur in the German Bight. Schrum (1997) showed how the spatial extent of thermohaline stratified areas, a precondition for the occurrence of tidal mixing fronts, depends on wind forcing possibly inducing differential advection. In a recent paper, Chegini et al. (2020) provided a more detailed analysis of different processes that affect stratification and destratification, including freshwater buoyancy input. Location of the Elbe River plume again depends on the wind driven residual circulation. Against this backdrop, it can be assumed that atmospheric forcing is also a key driver for the generation, movement and extinction of German Bight LCSs.

Although some patterns in the temperature (and salinity) field seem clearly related to ridges in the FTLE fields, it must nevertheless be noted that there is no one to one relationship. An example for this provides the rather smooth FTLE field in Fig. 2b. The corresponding temperature field (Fig. S4a) shows small-scale structures with less clear counterparts in the FTLE field. According to Fig. S4b, the Lagrangian divergence FDLD reproduces structures seen in the temperature field, but FDLD values are clearly smaller than those in Fig. 2b. Combining pure flow dynamics with a simple representation of the dynamics of temperature itself might be necessary for an explanation of these structures in the temperature field (Abraham and Bowen, 2002). Note that large divergences in coastal regions are likely to be artefacts because of water depths in tidal waters falling below the depth of the assumed 5 m surface layer (remember the same type of discrepancies also between Figs. 1b and 1c).

FTLE barriers may move, disappear or newly arise under changing environmental conditions. Numerical models are valuable tools for making observers aware of this fact. However, hydrodynamic models can never provide a perfect surrogate nature. In a comparative study, Hufnagl et al. (2017) found considerable discrepancies between the results from a large number of different North Sea tracer simulations essentially based on vertical mean currents. For surface drift simulations, additional simulation errors may arise from the necessity to specify the extent to which near surface currents are exposed to wave related Stokes drift or a direct wind drag. In field studies, corresponding parameters may be tuned empirically (e.g. Callies et al., 2017b). Altogether, simulated FTLE distributions will always be imperfect. Guo et al. (2016) propose concepts to extend the conventional analysis of deterministic FTLE fields and ridges to uncertain flow conditions. However, even in case of inaccurate simulations, the simulated FTLE would at least warn about key sensitivities of model output. If an observation is taken close to a simulated FTLE ridge, a simulated backward trajectory for this location must be used with due care.

https://doi.org/10.5194/os-2020-83
Preprint. Discussion started: 31 August 2020

This study did not address repelling LCSs in prediction mode. However, it is obvious that the above difficulties also occur when forward simulations are employed for search and rescue (Breivik et al., 2013), for instance. A forward FTLE field could possibly warn users against particularly sensitive dependences on the assumed location of numerical drift simulations. In tracer experiments, substantial model data discrepancies could result from just a slight misspecification of initial locations or a moderate displacement of simulated LCSs relative to reality.

5 Conclusions

The analysis of backward surface tracer simulations in the German Bight revealed the intermittent presence of linear structures (LCSs) across which the past history of water bodies substantially changes. Such sensitive dependences, represented by ridges in the fields of either backward FTLE or backward relative dispersion are potential sources of uncertainty in the interpretation of in situ observational data.

In the presence of repelling LCSs, large differences between observed and simulated tracer trajectories do not necessarily reflect poor model performance. If the location of a simulated LCS does not fully agree with reality, a tracer release point may come to lie on different sides of the separatrix in the model and in nature. In this case, a naive comparison of emerging trajectories could much exaggerate inconsistencies. The same arguments pertain to a comparison of different drift models. Conventional evaluations based on drift paths might be supplemented with a comparison of simulated FTLE fields that highlight spatial variability of prediction uncertainty.

Examples illustrated the variability of LCSs in the German Bight. For a more comprehensive picture it would be useful to establish a link between the recent history of atmospheric forcing, tidal movements and the main characteristics of the backward FTLE fields to be expected. Due to sometimes complex filamentary structures, a decomposition of FTLE fields in terms of a mean field plus the sum of a number of weighted anomaly fields (empirical orthogonal function analysis) seems not very promising. Classification of FTLE fields into a limited number of categories might be useful. This problem is left to future research.

Code and data availability. The hydrodynamic data analysed in this paper were obtained from the repository of the Federal Maritime and Hydrographic Agency (BSH). For access to the archived results of the operational hydrodynamical model BSHcmod, please contact BSH (www.bsh.de). The Lagrangian drift code PELETS is available on request from the author.

Video supplement. A video is provided (FTLE_2016.avi) that demonstrates the temporal development of FTLE fields in the course of the year 2016, based on FTLE fields calculated every 7 hours.

Author contributions. The author performed all analyses and prepared the manuscript.

https://doi.org/10.5194/os-2020-83
Preprint. Discussion started: 31 August 2020

Competing interests. The author declares that he has no conflict of interest.

Acknowledgements. Drift simulations were based on BSHcmod currents provided by the Federal Maritime and Hydrographic Agency (BSH). Graphs were produced using the Generic Mapping Tools software (GMT) available from www.soest.hawaii.edu/gmt/.

https://doi.org/10.5194/os-2020-83
Preprint. Discussion started: 31 August 2020

References

Abraham, E. R. and Bowen, M. M.: Chaotic stirring by a mesoscale surface-ocean flow, Chaos, 12, 373–381, https://doi.org/10.1063/1.1481615, 2002.

Aurell, E., Boffetta, G., Crisanti, A., Palatin, G., and Vulpiani, A.: Growth of noninfinitesimal perturbations in turbulence, Phys. Rev. Lett., 77, 1262–1265, https://doi.org/10.1103/PhysRevLett.77.1262, 1996.

Aurell, E., Boffetta, G., Crisanti, A., Palatin, G., and Vulpiani, A.: Predictability in the large: an extension of the concept of Lyapunov exponent, J. Phys. A, 30, 1–26, https://doi.org/10.1088/0305-4470/30/1/003, 1997.

Baschek, B., Schroeder, F., Brix, H., Riethmüller, R., Badewien, T. H., Breitbach, G., Brügge, B., Colijn, F., Doerffer, R., Eschenbach, C., Friedrich, J., Fischer, P., Garthe, S., Horstmann, J., Krasemann, H., Metfies, K., Merckelbach, L., Ohle, N., Petersen, W., Pröfrock, D., Röttgers, R., Schlüter, M., Schulz, J., Schulz-Stellenfleth, J., Stanev, E., Staneva, J., Winter, C., Wirtz, K., Wollschläger, J., Zielinski, O., and Ziemer, F.: The Coastal Observing System for Northern and Arctic Seas (COSYNA), Ocean Science, 13, 379–410, https://doi.org/10.5194/os-13-379-2017, https://www.ocean-sci.net/13/379/2017/, 2017.

Becker, G. A., Dick, S., and Dippner, J. W.: Hydrography of the German Bight, Mar. Ecol. Prog. Ser., 91, 9–18, 1992.

Beron-Vera, F. J., Olascoaga, M. J., Haller, G., Farazmand, M., Triñanes, J., and Wang, Y.: Dissipative inertial transport patterns near coherent Lagrangian eddies in the ocean, Chaos, 25, 087 412, https://doi.org/10.1063/1.4928693, 2015.

Branicki, M. and Malek-Madani, R.: Lagrangian structure of flows in the Chesapeake Bay, Nonlin Processes Geophys., 17, 149–168, https://doi.org/10.5194/npg-17-149-2010, 2010.

Breivik, Ø., Allen, A. A., Maisondieu, C., and Olagon, M.: Advances in search and rescue at sea, Ocean Dyn., 63, 83–88, https://doi.org/10.1007/s10236-012-0581-1, 2013.

Budéus, G.: Frontal variability in the German Bight, Sci. Mar., 53, 175–185, 1989.

Callies, U., Plüß, A., Kappenberg, J., and Kapitza, H.: Particle tracking in the Vicinity of Helgoland, North Sea: A Model Comparison, Ocean Dyn., 61, 2121–2139, https://doi.org/10.1007/s10236-011-0474-8, 2011.

Callies, U., Gaslikova, L., Kapitza, H., and Scharfe, M.: German Bight residual current variability on a daily basis: principal components of multi-decadal barotropic simulations, Geo-Mar. Lett., 37, 151–162, https://doi.org/10.1007/s00367-016-0466-2, 2017a.

Callies, U., Groll, N., Horstmann, J., Kapitza, H., Klein, H., Maßmann, S., and Schwichtenberg, F.: Surface drifters in the German Bight: model validation considering windage and Stokes drift, Ocean Sci., 13, 799–827, https://doi.org/10.5194/os-13-799-2017, 2017b.

Callies, U., Carrasco, R., Floeter, J., Horstmann, J., and Quante, M.: Submesoscale dispersion of surface drifters in a coastal sea near offshore wind farms, Ocean Sci., 15, 865–889, https://doi.org/10.5194/os-15-865-2019, 2019.

Chegini, F., Holtermann, P., Kerimoglu, O., Becker, M., Kreus, M., Klingbeil, K., Gräwe, U., Winter, C., and Burchard, H.: Processes of stratification and destratification during an extreme river discharge event in the German Bight ROFI, J. Geophys. Res.: Oceans, 125, e2019JC015 987, https://doi.org/10.1029/2019JC015987, 2020.

Chen, K., Ni, M., Cai, M., Huang, J. W. D., Chen, H., Wang, X., and Liu, M.: Optimization of a coastal environmental monitoring network based on the Kriging method: A case study of Quanzhou Bay, China, Biomed. Res. Int., 2016, Article ID 7137 310, https://doi.org/10.1155/2016/7137310, 2016.

Dick, S., Kleine, E., Müller-Navarra, S., Klein, H., and Komo, H.: The operational circulation model of BSH (BSHcmod). Model description and validation, Tech. Rep. 29/2001, BSH, 2001.

https://doi.org/10.5194/os-2020-83
Preprint. Discussion started: 31 August 2020

Dick, S., Kleine, E., and Janssen, F.: A new operational circulation model for the North Sea and Baltic Sea using a novel vertical coordinate setup and first results, in: Coastal to Global Operational Oceanography: Achievements and Challenges. Proceedings of the Fifth International Conference on EuroGOOS, 20-22 May 2008, Exeter, UK, edited by Dalhin, H., Bell, M. J., Flemming, N. C., and Petersen, S. E., 2008.

d'Ovidio, F., De Monte, S., Alvain, S., Dandonneau, Y., and Lévy, M.: Fluid dynamical niches of phytoplankton types, PNAS, 107, 18 366–18 370, https://doi.org/10.1073/pnas.1004620107, 2010.

d'Ovidio, F., Penna, A. D., Trull, T. W., Nencioli, F., Pujol, M.-I., Rio, M.-H., Park, Y.-H., Cotté, C., Zhou, M., and Blain, S.: The biogeochemical structuring role of horizontal stirring: Lagrangian perspectives on iron delivery downstream of the Kerguelen Plateau, Biogeosciences, 12, 5567–5581, https://doi.org/10.5194/bg-12-5567-2015, 2015.

Farazmand, M. and Haller, G.: Comuputing Lagrangian coherent structures from their variational theory, Chaos, 22, 013 128, https://doi.org/10.1063/1.3690153, 2012.

Günther, T. and Theisel, H.: Backward finite-time Lyapunov exponents in inertial flows, IEEE Trans. Vis. Comput. Graph., 23, 970–979, https://doi.org/10.1109/TVCG.2016.2599016, 2017.

Guo, H., He, W., Peterka, T., Shen, H.-W., Collis, S. M., and Helmus, J. J.: Finite-time Lyapunov exponents and Lagrangian coherent structures in uncertain unsteady flows, IEEE Trans. Vis. Comput. Graph., 22, 1672–1682, https://doi.org/10.1109/TVCG.2016.2534560, 2016.

Hadjighasem, A., Farazmand, M., Blazevski, D., Froyland, G., and Haller, G.: A critical coparison of Lagrangian methods for coherent structure detection, Chaos, 27, 053 104, https://doi.org/10.1063/1.4982720, 2017.

Haller, G.: Distinguished material surfaces and coherent structures in three-dimensional fluid flows, Physica D, 149, 248–277, https://doi.org/10.1016/S0167-2789(00)00199-8, 2001.

Haller, G.: A variational theory of hyperbolic Lagrangian coherent structures, Physica D, 240, 574–598, https://doi.org/10.1016/j.physd.2010.11.010, 2011.

Haller, G.: Lagrangian coherent structures, Annu. Rev. Fluid Mech., 47, 137–162, https://doi.org/10.1146/annurev-fluid-010313-141322, 2015.

Haller, G. and Yuan, G.: Lagrangian coherent structures and mixing in two-dimensional turbulence, Physica D, 147, 352–370, https://doi.org/10.1016/S0167-2789(00)00142-1, 2000.

Harrison, C. S. and Glatzmaier, G. A.: Lagrangian coherent structures in the California Current System - sensitities and limitations, Geophys. Astro. Fluid Dyn., 106, 22–44, https://doi.org/10.1080/03091929.2010.532793, 2010.

Hernández-Carrasco, I., Orfila, A., Rossi, V., and Garçon, V.: Effect of small scale transport processes on phytoplankton distribution in coastal seas, Scientific Reports, 8, 8613, https://doi.org/10.1038/s41598-018-26857-9, 2018.

Holt, J. and Umlauf, L.: Modelling the tidal mixing fronts and seasonal stratification of the Northwest European Continental shelf, Cont. Shelf Res., 28, 887–903, https://doi.org/10.1016/j.csr.2008.01.012, 2008.

Hufnagl, M., Payne, M., Lacroix, G., Bolle, L. J., Daewel, U., Dickey-Collas, M., Gerkema, T., Huret, M., Janssen, F., Kreus, M., Pätsch, J., Pohlmann, T., Ruardij, P., Schrum, C., Skogen, M. D., Tiessen, M. C., Petitgas, P., van Beek, J. K., van der Veer, H. W., and Callies, U.: Variation that can be expected when using particle tracking models in connectivity studies, J. Sea Res., 127, 133–149, https://doi.org/10.1016/j.seares.2017.04.009, 2017.

https://doi.org/10.5194/os-2020-83
Preprint. Discussion started: 31 August 2020

Huhn, F., von Kameke, A., Allen-Perkins, S., Montero, P., Venancio, A., and Pérez-Muñuzuri, V.: Horizontal Lagrangian transport in a tidal-driven estuary - Transport barriers attached to prominent coastal boundaries, Cont. Shelf Res., 39-40, 1–13, https://doi.org/10.1016/j.csr.2012.03.005, 2012.

Huntley, H. S., Lipphardt, B. L., Jacobs, G., and Kirwan Jr., A. D.: Clusters, deformation, and dilation: Diagnostics for material accumulation regions, J. Geophys. Res., 120, 6622–6636, https://doi.org/10.1002/2015JC011036, 2015.

James, I. D.: A three-dimensional numerical shelf-sea front model with variable eddy viscosity and diffusivity, Cont. Shelf Res., 3, 69–98, 1984.

Karrasch, D. and Haller, G.: Do finite-size Lyapunov exponents detect coherent structures?, Chaos, 23, 043 126, https://doi.org/10.1063/1.4837075, 2013.

Kim, N.-H. and Hwang, J. H.: Optimal design of water quality monitoring networks in semi-enclosed estuaries, Sensors, 20, 1498, https://doi.org/10.3390/s20051498, 2020.

Krause, G., Budeus, G., Gerdes, D., Schaumann, K., and Hesse, K.: Frontal systems in the German Bight and their physical and biological effects, in: Marine Interfaces Ecohydrodynamics, edited by Nihoul, J. C. J., pp. 119–140, Elsevier, Amsterdam, 1986.

LaCasce, J. H.: Statistics from Lagrangian observations, Prog. Oceanogr., 77, 1–29, https://doi.org/10.1016/j.pocean.2008.02.002, 2008.

LaCasce, J. H. and Ohlmann, C.: Relative dispersion at the surface of the Gulf of Mexico, J. Mar. Res., 61, 285–312, https://doi.org/10.1357/002224003322201205, 2003.

Lapeyre, G. and Klein, P.: Impact of the small-scale elongated filaments on the oceanic vertical pump, J. Mar. Res., 64, 835–851, https://doi.org/10.1357/002224006779698369, 2006.

Lehahn, Y., d'Ovidio, F., Lévy, M., and Heifetz, E.: Stirring of the northeast Atlantic spring bloom: A Lagrangian analysis based on multisatellite data, J. Geophys. Res., 112, C08 005, https://doi.org/10.1029/2006JC003927, 2007.

Lekien, F., Coulliette, C., Mariano, A. J., Ryan, E. H., Shay, L. K., Haller, G., and Marsden, J.: Pollution release tied to invariant manifolds: A case study for the coast of Florida, Physica D, 210, 1–20, https://doi.org/10.1016/j.physd.2005.06.023, 2005.

Lucas, J., Koester, I., Wichels, A., Niggemann, J., Dittmar, T., Callies, U., Wiltshire, K. H., and Gerdts, G.: Short-term dynamics of North Sea bacterioplankton-dissolved organic matter coherence on molecular level, Front. Microbiol., 7:321, https://doi.org/10.3389/fmicb.2016.00321, 2016.

Meyerjürgens, J., Ricker, M., Schakau, V., Badewien, T. H., and Stanev, E. V.: Relative dispersion of surface drifters in the North Sea: The effect of tides on mesoscale diffusivity, JGR Oceans, 124, e2019JC015925, https://doi.org/10.1029/2019JC015925, 2020.

Molcard, A., Andrew C, P., and Özgökmen, T. M.: Directed drifter launch strategies for Lagrangian data assimilation using hyperbolic trajectories, Ocean Model., 12, 268–289, https://doi.org/10.1016/j.ocemod.2005.06.004, 2006.

Olascoaga, M. J., Beron-Vera, F. J., Haller, G., Triñanes, J., Iskandarani, M., Coelho, E. F., Haus, B. K., Huntley, H. S., Jacobs, G., Kirwan Jr., A. D., Lipphardt Jr., B. L., Özgökmen, T. M., Reniers, A. J. H., and Valle-Levinson, A.: Drifter motion in the Gulf of Mexico constrained by altimetric Lagrangian coherent structures, Geophys. Res. Lett., 40, 6171–6175, https://doi.org/10.1002/2013GL058624, 2013.

Orre, S., Gjevik, B., and LaCasce, J. H.: Characterizing chaotic dispersion in a coastal tidal model, Cont. Shelf Res., 26, 1360–1374, https://doi.org/10.1016/j.csr.2005.11.015, 2006.

Peacock, T. and Haller, G.: Lagrangian coherent structures: the hidden skeleton of fluid flows, Phys. Today, 66, 41–47, https://doi.org/10.1063/PT.3.1886, 2013.

Peng, J. and Dabiri, J. O.: Transport of inertial particles by Lagrangian coherent structures: application to predator-prey interaction in jellyfish feeding, J. Fluid Mech., 623, 75–84, https://doi.org/10.1017/S0022112008005089, 2009.

https://doi.org/10.5194/os-2020-83
Preprint. Discussion started: 31 August 2020

Pierrehumbert, R. T. and Yang, H.: Global chaotic mixing on isentropic surfaces, J. Atmos. Sci., 50, 2462–2480, https://doi.org/10.1175/1520-0469(1993)050<2462:GCMOIS>2.0.CO;2, 1993.

Poje, A. C., Toner, M., Kirwan Jr., A. D., and Jones, C. K. R. T.: Drifter launch strategies based on Lagrangian templates, J. Phys. Oceanogr., 32, 1855–1869, https://doi.org/10.1175/1520-0485(2002)032<1855:DLSBOL>2.0.CO;2, 2002.

Press, W. H., Teukolsky, S. A., Vetterling, W. T., and Flannery, B. P.: Numerical Recipies in FORTRAN - The Art of Scientific Computing, Cambridge University Press, Cambridge, UK, 2 edn., 1992.

Sansón, L. Z., Pérez-Brunius, P., and Sheinbaum, J.: Surface relative dispersion in the southwestern Gulf of Mexico, J. Phys. Oceanogr., 47, 387–403, https://doi.org/10.1175/JPO-D-16-0105.1, 2017.

Sapsis, T. and Haller, G.: Inertial particle dynamics in a hurricane, J. Atmos. Sci., 66, 2481–2492, https://doi.org/10.1175/2009JAS2865.1, 2009.

Sapsis, T., Peng, J., and Haller, G.: Instabilities on prey dynamics in jellyfish feeding, Bull. Math. Biol., 73, 1841–1856, https://doi.org/10.1007/s11538-010-9594-4, 2011.

Scales, K. L., Hazen, E. L., Jacox, M. G., Castruccio, F., Maxwell, S. M., Lewison, R. L., and Bograd, S. J.: Fisheries bycatch risk to marine megafauna is intensified in Lagrangian coherent structures, PNAS, 115, 7362–7367, https://doi.org/10.1073/pnas.1801270115, 2018.

Schrum, C.: Thermohaline stratification and instabilities at tidal mixing fronts: results of an eddy resolving model for the German Bight, Cont. Shelf Res., 17, 689–716, https://doi.org/10.1016/S0278-4343(96)00051-9, 1997.

Schulz, J.-P. and Schättler, U.: Kurze Beschreibung des Lokal-Modells Europa COSMO-EU (LME) und seiner Datenbanken auf dem Datenserver des DWD, https://www.dwd.de/SharedDocs/downloads/DE/modelldokumentationen/nwv/cosmo_eu/cosmo_eu_dbbeschr_201406.pdf?__blob=publicationFile&v=3, 2014.

Shadden, S. C., Lekien, F., and Marsden, J. E.: Definition and properties of Lagrangian coherent structures from finite-time Lyapunov exponents in two-dimensional aperiodic flows, Physica D, 212, 271–304, https://doi.org/10.1016/j.physd.2005.10.007, 2005.

Shadden, S. C., Lekien, F., Paduan, J. D., Chavez, F. P., and Marsden, J. E.: The correlation between surface drifters and coherent structures based on high-frequency radar data in Monterey Bay, Deep-Sea Res. II, 56, 161–172, https://doi.org/10.1016/j.dsr2.2008.08.008, 2009.

Simpson, J. H. and Pingree, R. D.: Shallow sea fronts produced by tidal stirring, in: Oceanic Fronts in Coastal Processes, edited by Bowman, M. J. and Esaias, W. E., pp. 29–42, Springer, Berlin, https://doi.org/10.1007/978-3-642-66987-3_5, 1978.

Smith, S. and Banke, E.: Variation of the sea surface drag coefficient with wind speed, Q. J. Roy. Meteor. Soc., 101, 665–673, https://doi.org/10.1002/qj.49710142920, 1975.

Stanev, E. V., Schulz-Stellenfleth, J., Staneva, J., Grayek, S., Grashorn, S., Behrens, A., Koch, W., and Pein, J.: Ocean forecasting for the German Bight: from regional to coastal scales, Ocean Sci., 12, 1105–1136, https://doi.org/10.5194/os-12-1105-2016, 2016.

Sudharsan, M., Brunton, S. L., and Riley, J. J.: Lagrangian coherent structures and inertial particle dynamics, Phys. Rev. E, 93, 033 108, https://doi.org/10.1103/PhysRevE.93.033108, 2016.

Sündermann, J. and Pohlmann, T.: A brief analysis of the North Sea physics, Oceanologia, 53, 663–689, https://doi.org/10.5697/oc.53-3.663, 2011.

Thiel, M., Hinojosa, I. A., Joschko, T., and Gutow, L.: Spatio-temporal distribution of floating objects in the German Bight (North Sea), J. Sea Res., 65, 368–379, https://doi.org/10.1016/j.seares.2011.03.002, 2011.

Tian, F., He, Q., Liu, Z., and Chen, G.: Extracting Lagrangian coherent structures in the Kuroshio current system, Ocean Dyn., 69, 641–656, https://doi.org/10.1007/s10236-019-01262-6, 2019.

https://doi.org/10.5194/os-2020-83
Preprint. Discussion started: 31 August 2020

van Sebille, E., Griffies, S. M., Abernathey, R., Adams, T. P., Berloff, P., Biastoch, A., Blanke, B., Chassignet, E. P., Cheng, Y., Cotter, C. J., Deleersnijder, E., Döös, K., Drake, H. F., Drijfhout, S., Gary, S. F., Heemink, A. W., Kjellsson, J., Koszalka, I. M., Lange, M., Lique, C., MacGilchrist, G. A., Marsh, R., Mayorga Adame, C. G., McAdam, R., Nencioli, F., Paris, C. B., Piggott, M. D., Polton, J. A., Rühs, S., Shah, S. H., Thomas, M. D., Wang, J., Wolfram, P. J., Zanna, L., and Zika, J. D.: Lagrangian ocean analysis: Fundamentals and practices, Ocean Modelling, 121, 49 – 75, https://doi.org/10.1016/j.ocemod.2017.11.008, 2018.

Wiggins, S.: The dynamical systems approach to Lagrangian transport in oceanic flows, Annu. Rev. Fluid Mech., 37, 295–328, https://doi.org/10.1146/annurev.fluid.37.061903.175815, 2005.